Ionospheric Disturbances Triggered by China's Long March 2D Rocket

Youkun Wang, Yibin Yao, Jian Kong, and Lulu Shan

***Abstract*—Using the data of 382 ground global navigation satellite system (GNSS) network stations in Western China, we studied and analyzed the ionospheric disturbances triggered by the "Long March" 2D rocket launch in Jiuquan, China on December 3, 2017. As compared with previous research, a higher sampling resolution for GNSS data (with a frequency of 1 Hz) was used to obtain more accurate occurrence times and propagation velocities of ionospheric disturbances. By using a method based on a quadratic function of time to fit a raw total electron content (TEC) series, a filtered TEC series was calculated using carrier observations, and a two-dimensional disturbances map was drawn. A new method, which accounts for the flight time of the rocket, was used to calculate the velocity of the shock wave. Ionospheric depletions and the shock wave were observed after the launch of the rocket. The depletion was observed within 100 to 1000 km south of the launch site along the rocket trajectory, which had a maximum amplitude of ∼3.8 TEC units (TECU), reaching ∼56% of the background TEC. A shock wave of V-shaped disturbances with amplitudes of ∼0.67 TECU was detected on both sides of the rocket trajectory. The shock wave moved southeast at an average velocity of ∼1861 m/s at a location 2200 km away from the launch site. Ionospheric disturbances with distances of more than ∼3000 km from the launch site were also observed.**

***Index Terms*—Ionospheric depletion, ionospheric disturbances, rocket, shock wave.**

I. Introduction

OWING to certain physical factors such as the time, location, and magnitude of rocket launches, each rocket launch can be regarded as an active experiment for studying the ionosphere response [1]. Booker [2] first discovered the ionospheric disturbances caused by the launch of a Vanguard II rocket. Since then, ionospheric disturbances triggered by rockets, space shuttles, or missile launches have been studied, based on ionosondes [2], [3], incoherent scattering radar [4], and very long baseline interferometers [5]. With the establishment of a global satellite navigation system (GNSS), GNSS receiver networks have gradually become the primary means for medium and large scales ionospheric disturbances monitoring, owing to their high-resolution, all-weather abilities, and real-time characteristics, which can reflect the detailed structures of ionospheric disturbances. In recent years, many scholars have used ground GNSS receiver networks to analyze ionospheric responses to rocket launchs [6], [7], [8], [9], [10], [11], [12], [13].

Traveling ionospheric disturbances (TIDs) have been reported following numerous rocket launches, and reveal their characteristics within approximately 2000 km from the launch site. Calais and Minster [6] detected the shock wave signature of ionospheric disturbances following a space shuttle ascent using a single ground-based global positioning system (GPS) station. Afraimovich et al. [14] used a global international GNSS service (IGS) network to determine that the ionospheric response has the character of an N-wave, corresponding to the form of a shock wave as excited from launches of proton and space shuttle launch vehicles (LVs). A clear shock wave signature was also observed from a North Korea rocket launch, using the dense GPS networks in Japan [11]. Ding et al. [10] also found a V-shape shock acoustic wave excited by the launch of the long march 2F rocket using the dense GPS networks over China. These studies show that the TIDs generated by rocket launches are characterized by a V-shape shock wave signature near the trajectory, with horizontal velocities of 600–2500 m/s. In addition to the shock and acoustic waves, Lin et al. [15] and Liu et al. [12] found concentric TIDs (CTIDs) triggered by the launch of a SpaceX Falcon 9 rocket and China's Long March 4B rocket.

In addition to TIDs and CTIDs, ionospheric electron density depletion is another ionospheric disturbance excited by a rocket's blast plume, via interactions between perturbed neutral particles and ionized components [16]. Ozeki and Heki [9] found ionospheric holes caused by ballistic missiles from North Korea, as detected with a dense Japanese GPS array. Choi and Kil [17] used GNSS stations in South Korea to detect the large ionospheric total electron content (TEC) depletion induced by a 2016 North Korean rocket. Liu et al. [12] observed an ionospheric depletion excited by two launches of the Long March 4B rocket that carried "China-Brazil Earth Resources Satellite 3" and "China-Brazil Earth Resources Satellite 4," respectively. These studies show that the TEC series shows an evident decrease several minutes after the launch of the rocket. The TEC depletion can reach ∼50% of the background TEC, and can last 1–2 h.

Manuscript received 24 June 2022; revised 21 November 2022; accepted 13 January 2023. Date of publication 23 January 2023; date of current version 6 February 2023. This work was supported by the National Natural Science Foundation of China under Grant 41874033, Grant 42142037, Grant 41941010, and Grant 41721003, in part by the General fund project of Hubei Province under Grant 2020CFB603, and in part by the project supported by the Open Fund of Hubei Luojia Laboratory under Grant 220100046. *(Corresponding author: Yibin Yao.)*

Youkun Wang and Lulu Shan are with the School of Geodesy and Geomatics, Wuhan University, Wuhan 430072, China (e-mail: beanflower@whu.edu.cn; llshan@whu.edu.cn).

Yibin Yao is with the School of Geodesy and Geomatics, Wuhan University, Wuhan 430072, China, and also with Luojia Laboratory, Wuhan 430079, China (e-mail: ybyao@whu.edu.cn).

Jian Kong is with the Chinese Antarctic Center of Surveying and Mapping, Wuhan University, Wuhan 430079, China, and also with Luojia Laboratory, Wuhan 430079, China (e-mail: jkong@whu.edu.cn).

Digital Object Identifier 10.1109/JSTARS.2023.3238867

In this article, the ionospheric disturbances triggered by the launch of the long march two-dimensional (LM-2D) rocket are analyzed for the first time, using the dense ground GNSS network in China. From this launch event, we observed two different types of ionospheric disturbances: ionospheric depletions and shock waves. The ionospheric depletion main appeared at 300 to 400 km away from the launch site, and the maximum amplitude of the depletion can reduce 56% of the background value of the TEC. The ionospheric shock waves clearly appeared after the rocket launch along the rocket trajectory, even 3000 km far away from the launch site, and its average velocity can reach ∼1861 m/s.

II. Event Information and Data Processing

A. Event Information

The LM-2D is a two-stage carrier rocket, and is mainly used for launching low-earth orbit (LEO) and sun synchronous orbit (SSO) satellites. At 04:11 universal time (UT) [local time (LT) = UT + 8] on December 3, 2017, an LM-2D LV successfully launched the "Land Survey Satellite-1" (LKW-1) at the Jiuquan Satellite Launch Center (40.96°N, 100.29°E, red star in Fig. 1).

Fig. 1 also shows the projection (blue line) of the rocket's approximate flight trajectory on the ground, according to the Federal Aviation Administration (https://pilotweb.nas.faa.gov/Pilot-Web/). After launching, the rocket flew southwest with an azimuth (clockwise from North) of the trajectory at approximately 194°, passing through Myanmar, the Bay of Bengal, and the Andaman and Nicobar Islands, and finally entering the Indian Ocean. The rocket traveled southwest for more than 3000 km, reaching an apogee of 500 km altitude, achieved a velocity of more than 7 km/s, and sent the spacecraft to a LEO of 488 by 504 kilometers, inclined at 97.46°. The LV completed its flight sequences, including first/second stage separation, fairing jettison, 2nd stage main engine shut down, 2nd stage vernier engine shut down, and spacecraft / LV separation at $t0 + 154$ s, $t0 + 184$ s, $t0 + 328$ s, $t0 + 620$ s, and $t0 + 637$ s, respectively, after the LV lifted off at 04:11 UT ($t0$).

B. Data Processing

The GNSS data used in this article are mainly obtained from the Crustal Movement Observation Network in China, the Satellite Navigation and Positioning Reference Station System of Yunnan Province and Qinghai Province in China, and the GNSS networks provided by the IGS. After analysis and data preprocessing, the datum of 382 stations is selected for analysis in this article. The geographical locations of the GNSS stations are shown in Fig. 1. To obtain more accurate characteristics of ionospheric disturbances, we adopted a higher time resolution data (1 s) from the GNSS stations.

First, the carrier phase observations and pseudo-range observations of the GNSS stations are subjected to preprocessing, such as cycle slip detection and repair, to obtain "clean" data. Then, using the GNSS dual-frequency observation data, a carrier phase smoothing method is used to calculate the slant TEC (sTEC). Based on a thin-layer ionosphere assumption, a

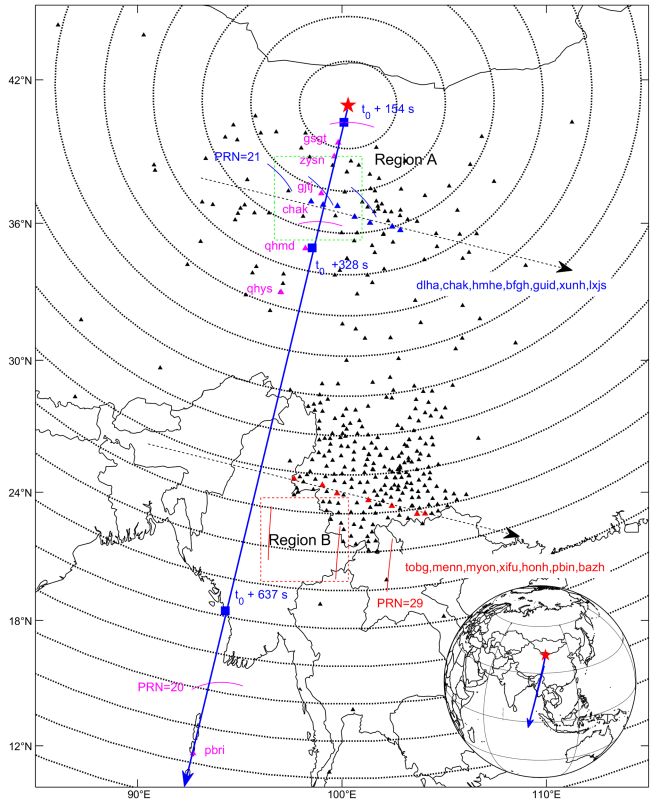

Fig. 1. Location of GNSS sites and the trajectory of the LM-2D. Specifically, triangles stand for GNSS sites (black). Some of them (pink) are along the rocket trajectory, while some are perpendicular to the rocket trajectory (blue and red). The blue and red are 480 and 1800 km from the launch site, respectively. The solid lines in pink, blue, and red represent the trajectories (only the trajectories observed from the first and last stations are drawn) of ionospheric pierce points (IPPs). The blue solid boxes show the general positions of the rocket at some key epoch. The green rectangle covers the GNSS stations of the G29 satellite IPPs (region A), while the red rectangle covered the other IPPs (region B) of the same satellite. It also implicates the Jiuquan Satellite Launch Center (red star), and the projection of the rocket ground track (blue arrow).

modified single-layer mapping function is used to convert the sTEC into a vertical TEC (vTEC). The thin-layer ionosphere altitude and the elevation cutoff are set to typical values of 300 km [9] and 30°, respectively. To analyze the characteristics of the ionospheric depletion, we used a second-order polynomial method to fit the original vTEC series using (1), and estimated the values for *a, b,* and *c* using a least-squares method with 30 min of period data, before the rapid decrease of vTEC series. Then, we used (1) to calculate the value of the fitting TEC series, and the vTEC anomaly was the fitting TEC series minus the raw TEC series

$$v\mathrm{TEC}(t) = at^2 + bt + c. \tag{1}$$

Fig. 2(a) shows the raw and ploy fit TEC series of the station "qhmd," as received by satellite G20. The blue solid line and the red solid line represent the raw vTEC series and the ploy fit vTEC series, respectively. An unusual TEC decrease with an amplitude of ∼3 TEC units (TECU) appeared 5 min after the launch of the rocket. After nearly two hours, the TEC value gradually returned to normal.

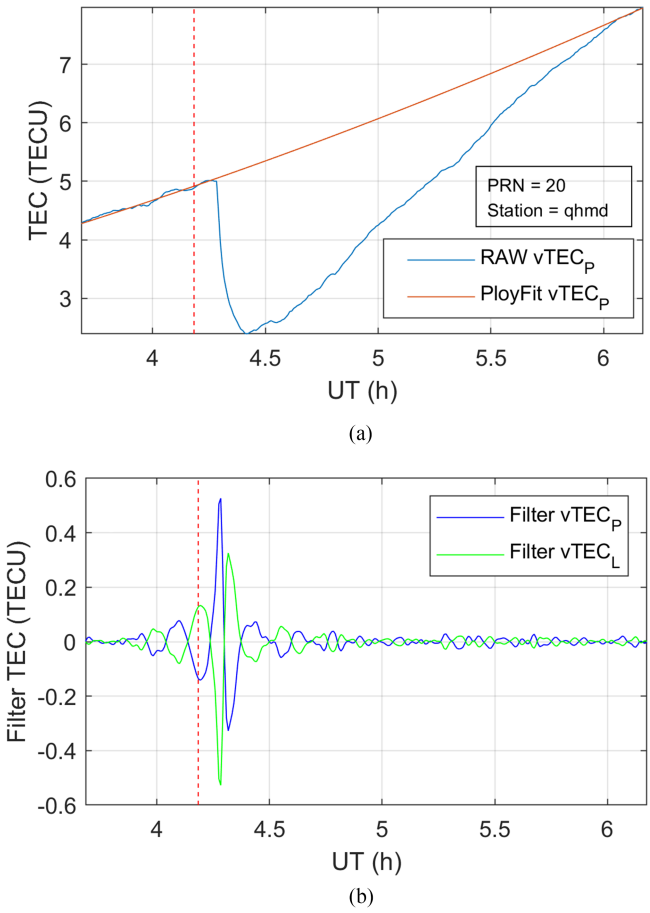

Fig. 2. Raw TEC series, ployfit TEC series, and filter TEC series of station "qhmd," as received by satellite G20. (a) Blue solid line is the raw vTEC series; the red solid line is the ployfit vTEC series; and the red dotted line marks the time of launch. (b) Blue solid line represents the filter series of $\mathrm{v}TEC_P$. The green solid line represents the filter series of $\mathrm{v}TEC_L$.

Usually, dual-frequency GPS data with a time resolution of 30 s is used to study ionospheric disturbances, which has an error of $\pm$ 30 s in abnormal times, and larger noise in a vTEC series. Here, only the carrier phase observations with 1 s resolution are used to calculate the disturbance TEC (dTEC), to obtain more accurate characteristics of the ionospheric disturbances using (3)

$$s\mathrm{TEC}_P = -\frac{\left(f_1^2 f_2^2\right)}{40.28\left(f_2^2 - f_1^2\right)}\left(P_1 - P_2 - \varepsilon_P\right) \tag{2}$$

$$s\mathrm{TEC}_L = \frac{\left(f_1^2 f_2^2\right)}{40.28\left(f_2^2 - f_1^2\right)}\left(L_1 - L_2 - \varepsilon_L\right). \tag{3}$$

Here, sTEC is the slant TEC, $L1$ and $L2$ are the GNSS phase measurements, $P1$ and $P2$ are the GNSS code measurements, f1 and f2 are the frequencies of the GNSS ($f1 = 1575.42$ MHz and $f2 = 1227.60$ MHz), ε_P is the sum of the hardware delay and observed noise for a pseudorange observation, and ε_L is the sum of the ambiguity of the carrier phase observation, hardware delay, and observed noise ε_P and ε_L are regarded as constants during the calculation.

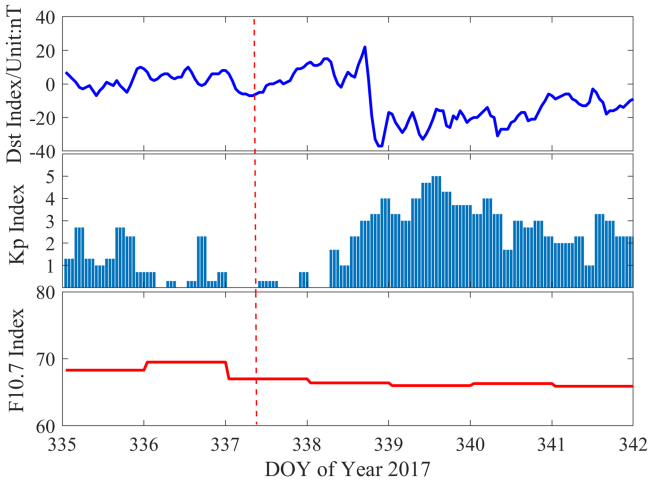

Fig. 3. Variations of geomagnetic conditions during December 1–7, 2017. The red dotted line marks the time of launch.

We applied a zero-phase sixth-order finite impulse response Butterworth filter, with cutoffs at 2 and 12 min, to determine the sTEC_L. The constant terms ε_P and ε_L can be estimated by (2) and (3). Then, we converted the fitting sTEC to a vTEC. As shown in Fig. 2(b), the filter vTEC_P and the filter vTEC_L are approximately equal in size and opposite in sign, and have X-axis symmetry. Fig. 2(b) shows that the times of the maximum amplitude of the filter vTEC_P and filter vTEC_L values are at 330 and 324 s after launch, respectively. The maximum amplitudes are 0.53 TECU and -0.51 TECU, respectively. Therefore, the inverse sign of the vTEC_L series can be used to analyze and obtain more accurate characteristics of the ionospheric disturbances.

III. Observations

A. Shock Wave Propagation

Fig. 3 shows the variation of the disturbance storm time (Dst) index, *Kp* index, and F10.7 index, covering from day-of-year (DOY) 335 to DOY 342 in 2017. The geomagnetic conditions are quiet on the day of the rocket launch (DOY 337), and the *Kp* index is 0 at 8:00 UT The average value of the Dst index for 24 h is 2, and the F10.7 index is within -0.1% of its mean value (from DOY 335 to 342). Therefore, we can eliminate the influences of geomagnetic and solar activity on the ionospheric disturbances of the rocket.

We chose 21 GNSS stations in different regions to analyze the different characteristics of ionospheric disturbances. Fig. 4 presents the TEC perturbation series of satellite G20 [see Fig. 4(a)], G21 [see Fig. 4(b)], and G29 [see Fig. 4(c)] observed from seven GNSS stations, respectively. All amplitudes of the perturbations are greater than the TEC series at the same time on the day before and after the launch. Thus, it can be determined that these ionospheric disturbances are excited by the rocket launch.

Fig. 4(a) shows the TEC perturbation series for the seven stations (see Fig. 1, pink triangles) close to the rocket's north-south trajectory. The first wave peaks of the TEC perturbation series are reached at 285, 204, 261, 279, 324, 426, and 660 s after

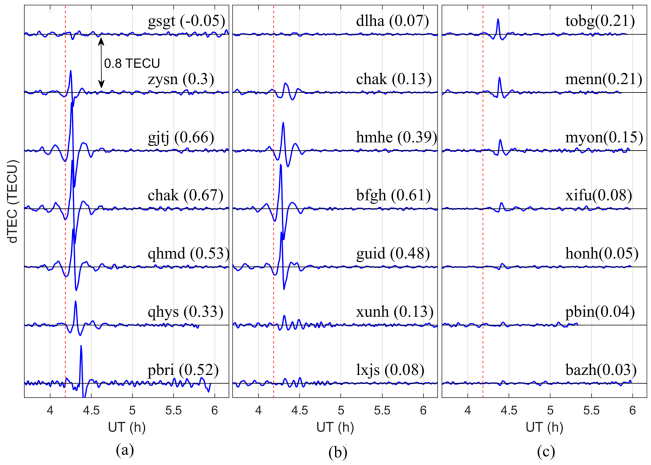

Fig. 4. dTEC series of satellite (a) G20, (b) G21, and (c) G29. The red dotted line indicates the launch time of the rocket, and the blue solid line represent the dTEC after vTEC filtering. The "zysn (0.3)" stands for the amplitude (0.3) of the first wave peak of the disturbance series observed from site zysn.

launch, and the amplitudes reach −0.05, 0.3, 0.66, 0.67, 0.53, 0.33, and 0.52 TECU, respectively. When these TEC series begin to have perturbations, they exhibit an N-shaped signature (except for the station gsgt), with a maximum amplitude of ∼0.67 TECU. The first and last stations with positive perturbations are station zysn and pbri, respectively, and the IPPs are located 140 km and 3000 km south of the launch site, respectively. Although the station pbri is the farthest from the launch site, its perturbation amplitude still reaches ∼0.52 TECU.

Fig. 4(b) shows the TEC perturbation series observed from seven stations (see Fig. 1, blue triangles) 480 km away from the launch site from the west to the east, i.e., perpendicular to the trajectory. The first wave peaks of the TEC perturbation series are reached at 515, 475, 387, 270, 311, 432, and 463 s after the launch, and the amplitudes reach 0.07, 0.13, 0.39, 0.61, 0.48, 0.13, and 0.08 TECU, respectively. The maximum amplitude of the TEC perturbations of other stations decreases gradually from the center of the station bfgh to the east-west side, and the time of its maximum amplitude gradually increases from the east-west side. The periodic oscillation perturbations after the N-shaped perturbation at the station xunh and lxjs, on the east side of the rocket trajectory, are more evident than those at other stations.

Fig. 4(c) shows the dTEC series for seven stations (see Fig. 1, red triangles) 1800 km away from the launch site from the west to the east, i.e., perpendicular to the trajectory. The first wave peaks of the TEC perturbation series are reached at 629, 696, 724, 773, 807, 850, and 864 s after the launch, and the amplitudes reach 0.2, 0.2, 0.15, 0.08, 0.05, 0.04, and 0.03 TECU, respectively. The locations of the IPPs with the maximum amplitude of the station tobg are closest to the trajectory, and the amplitudes of other stations gradually decrease from west to east. The time of the maximum amplitude appears to gradually increase from west to east.

As the IPPs are farther from the trajectory, the amplitude of the perturbation is gradually reduced to the noise level of the TEC signal (∼0.03 TECU). The aforementioned results indicated that the closer the location of the IPPs to the trajectory, the larger the amplitude of the first wave peak of the perturbation, and the shorter the time after the launch of the rocket. The perturbation presents as N-shaped signature (the maximum amplitude can reach ∼0.67 TECU), followed by a periodic oscillation (the amplitude ranges from 0.05 to 0.1 TECU). This indicates that the ionospheric disturbances are generated near the rocket trajectory, and then gradually spread to the east and west sides of the rocket trajectory before disappearing.

2-D maps of TEC perturbations have extensive used to analyze the characteristics of the ionospheric disturbances [18], [19], [20]. Fig. 5 shows 2-D TEC perturbation maps for the variation and position distribution during the period from 180 s to 990 s after the launch of the rocket at an interval of 30 s, and clearly shows the dynamic processes of the ionospheric disturbances in time and space. After the launch of the rocket and 180 s, a positive perturbation began to appear in the launch site along 140 km south of the rocket trajectory, with a maximum amplitude of 0.26 TECU. From 210 s to 360 s, the positive perturbations are concentrated in the area 300–500 km away from the launch site, and the ionospheric disturbance range gradually expands along the rocket trajectory to the east and west sides, with an amplitude of ∼0.67 TECU. From 360 s, i.e., 180 s after the occurrence of the positive perturbation, a negative perturbation begins to appear 140 km south of the launch site, and with the passage of time, the range of the ionospheric disturbances gradually spreads around the rocket trajectory. From 450 to 750 s, the positive perturbation propagates to 1600 km to 2000 km south of the launch site along the trajectory, and to the southeast. Similarly, after ∼200 s of the positive perturbation, i.e., 750 to 990 s after launch, the negative perturbation appears 2000 km south of the launch site along the trajectory, and propagates to the southeast. The amplitude of the perturbation gradually decreases, until it disappears.

By analyzing the propagation trend of the ionospheric disturbances as shown in Fig. 5, the shock wave first appeared 210 s after rocket launch near the launch site, and an obvious V-shaped shock wave gradually appeared 390s after rocket launch along the rocket trajectory at 300 to 700 km south of the rocket launch site. The shock wave with evident positive and negative phase structure characteristics gradually propagated southeast at 1800km away from the launch site. In the process of its propagation to a perpendicular distance of 600 km from the trajectory, the amplitude of the disturbance gradually decays until it disappears, and its duration can reach 990 s+ after the launch of the rocket [see plot (28) in Fig. 5].

To further analyze the propagation characteristics of the ionospheric disturbances, a time distance map is plotted as a function of the perpendicular distance of the IPPs to the rocket trajectory, and the time of the IPPs for two regions. The results of Fig. 6(a) and (b) were calculated using the IPPs of region A and region B (see Fig. 1), respectively. The method for calculating the propagation velocity uses the distance perpendicular to the trajectory [10]. Fig. 6(a) shows that the shock wave can be observed on both sides of the rocket trajectory. The maximum distance of the ionospheric disturbances to the west and east is ∼300 km. The propagation velocity of the shock wave is 835

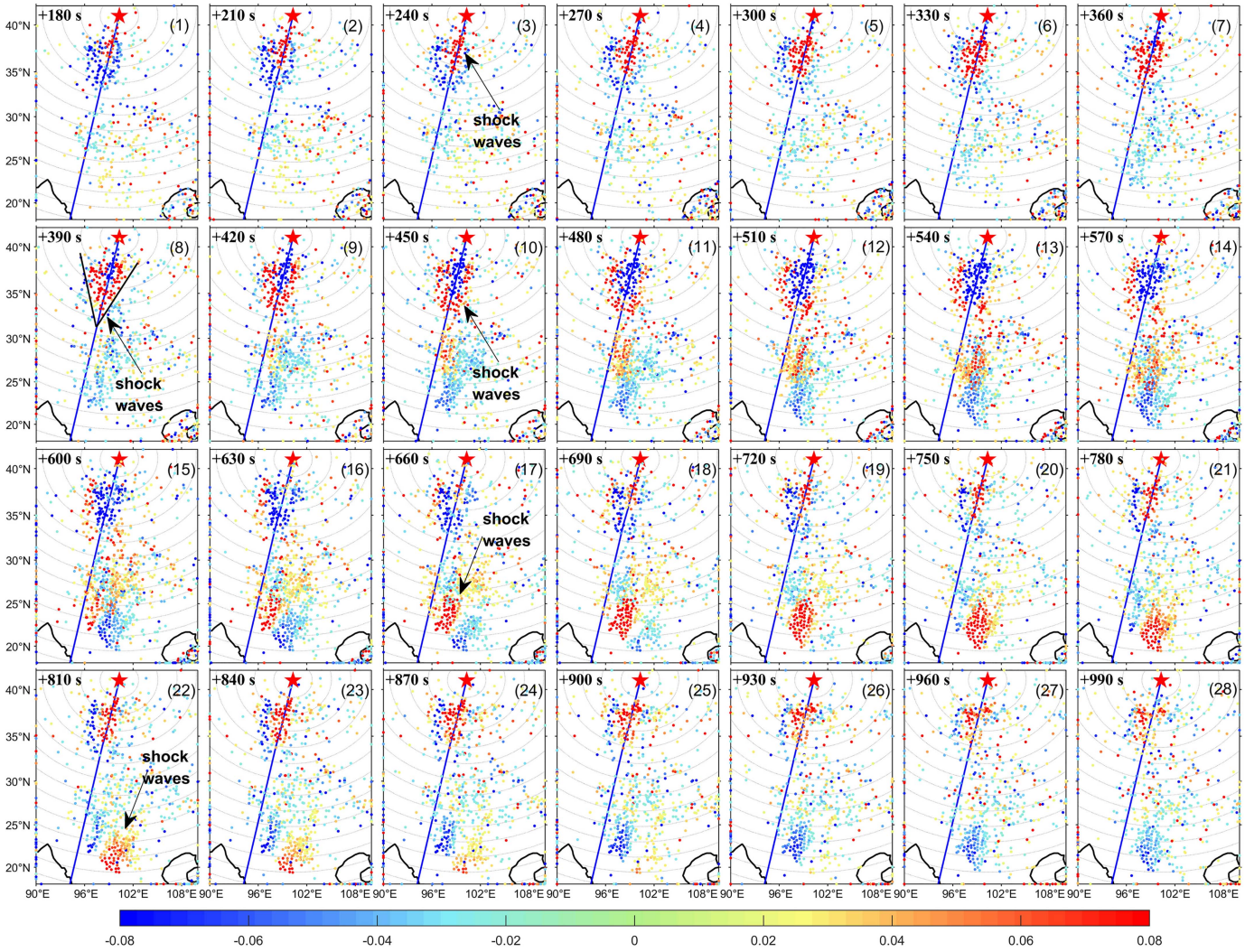

Fig. 5. 2-D maps of TEC perturbations during the launches. The solid color points represent the geographical locations of the maximum amplitude of the corresponding station IPPs, and the colors represent the TEC perturbation amplitudes, in units of TECU. Other symbols have the same meaning with the Fig. 1.

and 973 m/s to the west and east, respectively. The velocity of the waves gradually decreases as the waves move away from the rocket. Fig. 6(b) shows that the shock wave can only be observed on the east side of the rocket track, as there are no IPPs on west of the trajectory. The maximum distance of the eastward propagation of the ionospheric disturbances is ∼750 km, and the propagation velocity of the waves is 2211 m/s (without considering the rocket velocity). Fig. 6(a) shows that the duration of the ionospheric disturbances is longer than the result shown in Fig. 6(b), which is consistent with the results shown in Figs. 4 and 5.

To obtain the excitation source and more accurate propagation velocity of the shock wave, high sampling data of 1 s is used to analyze. We selected the locations and occurrence times of the largest perturbations (IPPs) of the same satellite, close to the rocket track in region B (see Fig. 1). Here, the ionospheric disturbances are more evident and the IPPs are more dense, which is useful for calculating and analyzing. The propagation velocity of the shock wave is calculated according to the way the excitation source directly propagates to the IPPs [6]. Fig. 7 shows a schematic diagram of the rocket's flight, as well as the shock wave propagating from the excitation source to the IPPs. It clearly shows the process of the shock wave generated during the rocket launch.

Based on the assumption that the shock wave was excited by the rocket's supersonic speed movement [10] and propagated from the source to the IPPs [6], we design three calculation schemes for analyzing the excitation sources of the ionospheric disturbances, and calculate the propagation velocity of the shock wave.

In scheme 1, it is considered that there is only one excitation source, located at a certain point on the rocket trajectory. As is shown in Fig. 8(a), R_0 is the excitation source of all IPPs (P_i), the time of the first largest perturbation of point P_0 is t_0, the time of the first largest perturbation of point P_i is t_i, and S_i is the distance from the excitation source to the IPPs (P_i). The propagation speed V_i of the shock wave can be calculated according to (4). Starting from the perpendicular foot F_0, the excitation source searches along the trajectory of the rocket toward the launch site in 10 km steps. The average velocity with the lowest standard

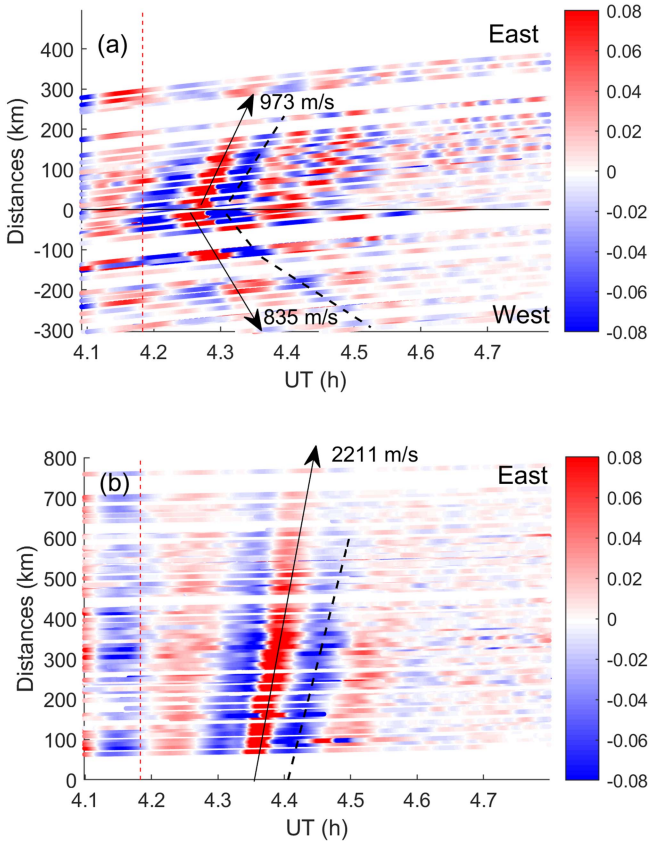

Fig. 6. TEC perturbative variation with the UT and propagation distance. Subfigures (a) and (b) are the dTEC series observed from stations located 480 km away from the launch site and perpendicular to the rocket trajectory (G21), and located 1800 km away from the launch site and perpendicular to the rocket trajectory (G29), respectively. The slope of the black arrow and black dotted line represents the propagation velocity of the shock wave and acoustic wave, respectively.

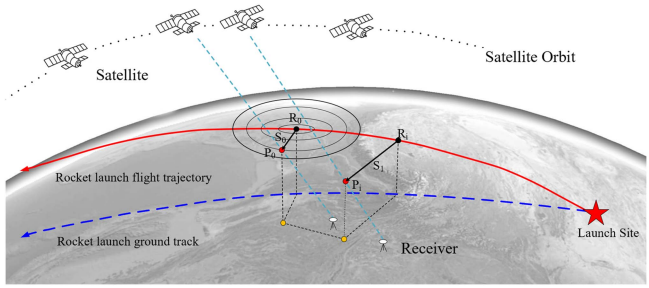

Fig. 7. Schematic of rocket flight and shock (acoustic) wave propagation. The black dots (R_i) are the positions of the excitation sources according to the positions of the IPPs (P_i). Red dots represent the maximum amplitudes of the dTEC series; R_0 is the excitation source according to the closest IPP (P_0) to the rocket's trajectory. S_i is the propagation distances from the excitation sources (R_i) to the IPPs (P_i) with the maximum amplitude of the dTEC series.

deviation of each velocity is taken as the propagation velocity of the shock wave

$$V_i = \frac{s_i - s_0}{t_i - t_0}. \tag{4}$$

In scheme 2, there are multiple excitation sources, and the excitation source is the perpendicular foot of the IPPs in the rocket trajectory [see Fig. 8(b)]. As the excitation source is assumed to be the perpendicular foot of the IPPs in the rocket trajectory, the speed of the shock wave can be calculated directly according to (4), without searching for the excitation source.

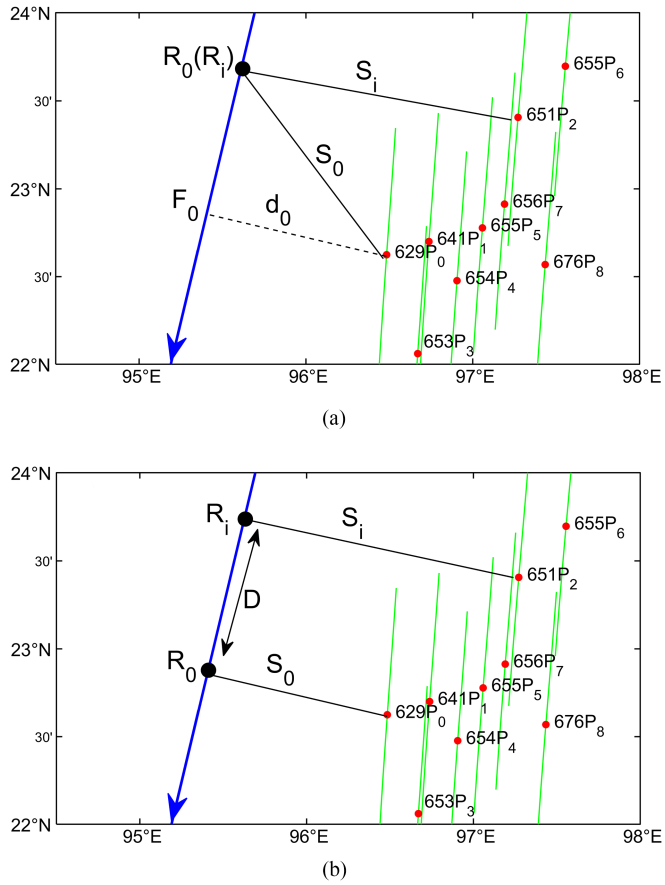

Fig. 8. Schematic for calculation of propagation velocity of shock waves. (a) Only one pair of excitation sources (R_0 and R_i) coincide, and R_0 and R_i are excitation sources of different IPPs. The blue arrow is the launch direction of the rocket track; the green solid line is the IPPs track of G29; the red dot is the position of the maximum amplitude of the dTEC series; S_i is the propagation distances from the excitation source to IPPs with the maximum amplitudes of the dTEC series. P_i indicates the IPP number (sorted by time) of the maximum amplitude of the dTEC series after launch. For example, the term "$629P_0$" indicates the first point with the maximum amplitude of the dTEC series at 629 s after the rocket launch. The black dots are the excitation sources corresponding to P_i, respectively. S_i is the propagation distances from the excitation sources to P_i. F_0 is the perpendicular foot of P_0 on the rocket trajectory. (b) Multiple excitation sources, and R_0 and R_i do not coincide. D is the projection distance of different IPPs in the rocket trajectory direction. Other symbols have the same meaning as in (a).

In scheme 3, a special case is considered, i.e., the rocket flight time in scheme 2. The flight distance D is approximately equal to the projection of the distance between the IPPs perpendicular to the rocket trajectory. Assuming that the velocity of the rocket is V_r, the speed of the shock wave can be calculated directly, according to

$$V_i = \frac{s_i - s_0}{t_i - t_0 + D/V_r}. \tag{5}$$

Fig. 9(a) shows the standard deviation of the shock wave propagation velocity, as calculated by scheme 1, scheme 2, and scheme 3 for region B, respectively. The black solid line, blue

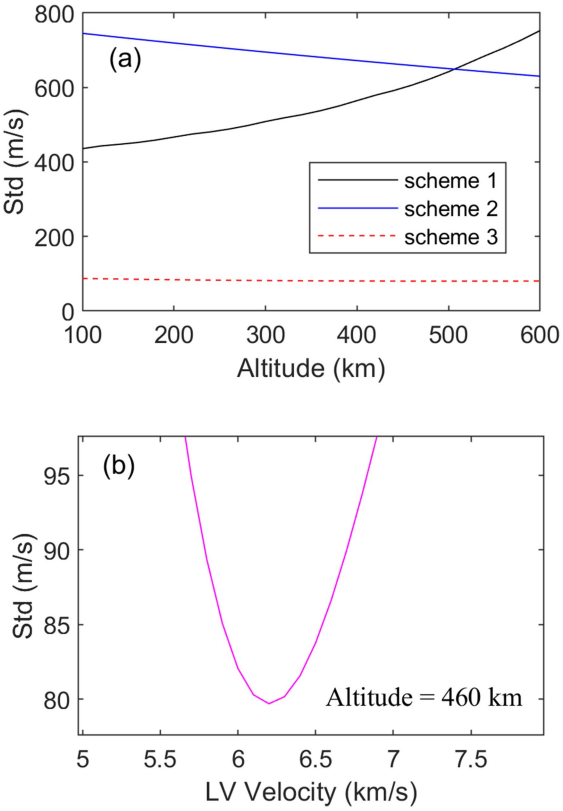

Fig. 9. Calculation of propagation velocity of shock waves. (a) Shock wave propagation velocity results for three schemes in region B. (b) Search map of rocket speed at 460 km altitude of IPPs in scheme 3, for region B.

solid line, and red dotted line represent the standard deviation results for the velocity calculated in scheme 1, scheme 2, and scheme 3, respectively. The altitude of the IPPs is calculated according to an interval of 100–600 km and a step length of 20 km. Fig. 9(a) shows that the minimum standard deviation of the shock wave propagation speed in schemes 1 and 2 is over 400 m/s in the range of 100–600 km, whereas the difference in the shock wave propagation speed as calculated in scheme 3 is not significant at different IPPs altitudes, and the standard deviation of the speed at 460 km reaches the minimum (±80.1 m/s). In (5), the velocity V_r of the rocket is unknown. Taking a rocket velocity of 5–8 km/s as the range, and searching in steps of 0.1 km/s, the propagation velocity V_i can be calculated. Fig. 9(b) shows that the standard deviation of the shock wave propagation velocity, as calculated using different rocket speeds, is the smallest when the rocket speed is 6.3 km/s, and the average speed of the shock wave is 1861 m/s when the IPPs altitude set to 460 km.

Fig. 9 shows that the bias of the propagation velocity of the shock wave in region B is minimum in scheme 3. Therefore, the results are supported to the shock wave may be the multi-point excitation from the rocket motion and the calculation of the propagation velocity must consider the rocket velocity.

B. Ionospheric Depletion

Fig. 10(a)–(c) shows the TEC series of satellites G20, G21, and G29 observed from seven stations, respectively. Fig. 10(a)

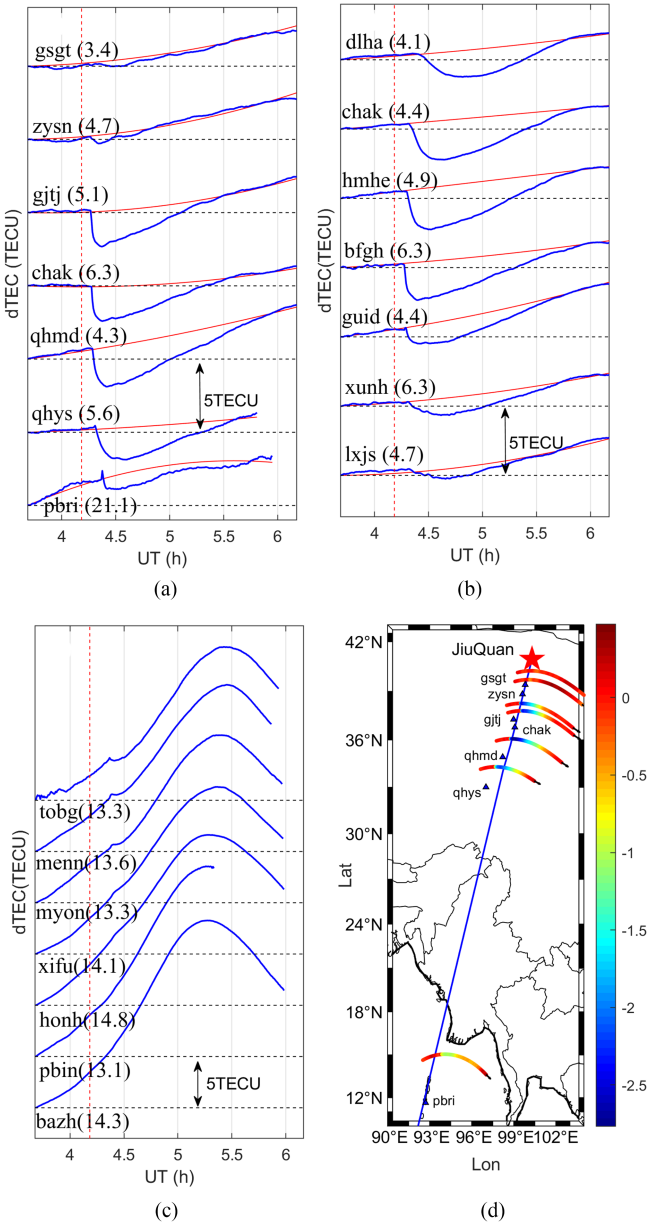

Fig. 10. Schematic diagram of depletion. (a)–(c) are the vTEC series of satellites G20, G21, and G29. The red dotted line marks the time of launch. The blue solid line is the raw vTEC series, and the red solid line is the fitting sequence $v\mathrm{TEC}_{\mathrm{fit}}$. (d) Geographical location distribution and IPPs tracks of seven stations along the rocket trajectory.

illustrates the TEC series observed from stations along the rocket trajectory, whereas Fig. 10(b) and (c) illustrate the TEC series observed from stations 480 and 1800 km away from the launch site and perpendicular to the rocket trajectory, respectively. The red dotted line denotes the rocket launch time, the blue solid line denotes the raw vTEC series, and the red solid line denotes the fitting vTEC series, as calculated by (1). Fig. 10(a) shows that the depletion appeared evidently from the station gjtj, and reached a maximum of ∼3.6 TECU at the station qhmd, before gradually decreasing to ∼1.1 TECU at the station pbri 3000 km away from the launch site. Fig. 10(d) shows the distributions and sizes of the depletions of the seven stations along the rocket

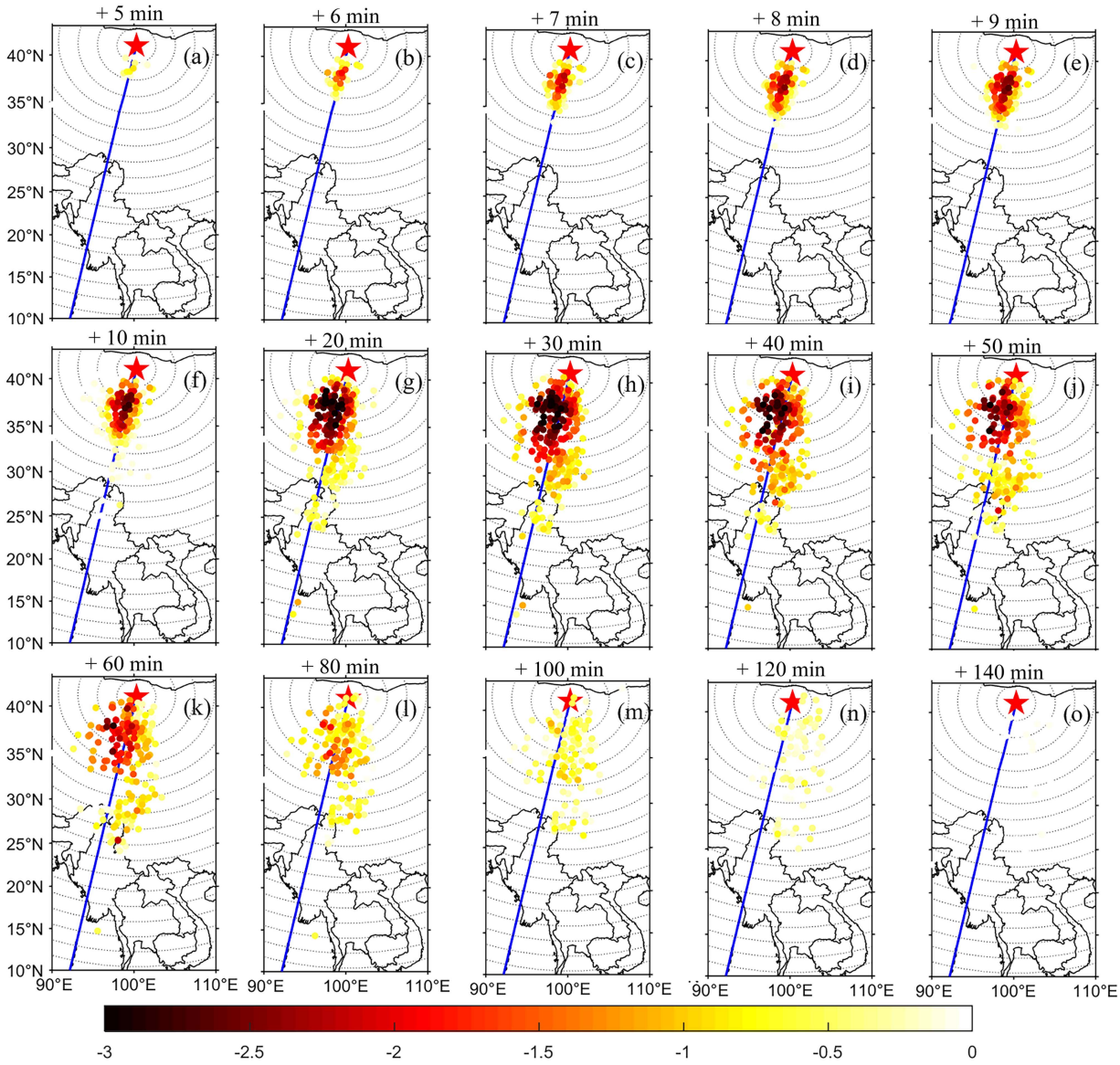

Fig. 11. 2-D depletion TEC maps between 5 and 140 min after launch. The solid color points are the geographical locations of the corresponding IPPs, and the color represents the magnitude of the depletion, in TECU.

launch trajectory. It clearly reflects that the depletion changes from small to large, then from large to small. Fig. 10(b) shows that the amplitude of the depletion reaches the maximum value near the trajectory, and decreases farther from the trajectory. Fig. 10(c) shows that there is almost no depletion in the TEC series of these stations. Perpendicular to the trajectory, Fig. 10(c) also clearly shows that the depletion near the trajectory reaches the maximum, and that the depletion gradually spreads to both sides and decreases.

Fig. 11 shows a 2-D snapshot of the space depletion distribution (with intervals of 1, 10, and 20 min) from 5 to 140 min after the launch, clearly indicating the dynamic change process of the dTEC with time and space. Five min after the launch, the TEC depletion first appears, 300 km south of the launch site [see Fig. 11(a)]. The depletion area gradually expands mainly around the rocket launch track, 200–800 km away from the launch site [see Fig. 11(a)–(h)]. From 30 to 40 min after the launch, the range of the depletion distribution reaches a maximum, covering between 100 and 1000 km away from the launch site along the trajectory, and the width is ∼300 km perpendicular to the trajectory (and is almost symmetrical to the trajectory). The depletion is mainly concentrated in the range of 400 to 600 km south of the rocket launch site. The amplitude of depletion reaches the maximum at ∼3.8 TECU. For 40 min after the launch of the rocket, the depletion range gradually narrowed down until it subsided, and the entire process lasted ∼2 h. In that regard, 120 min after launch, the depletion could hardly be observed.

IV. Discussion and Conclusion

A. Shock Wave

According to the rocket flight video and GNSS observation data of the rocket launch site, Fig. 12(a) draws the relationship diagram of the rocket's flight time, flight height (blue curve), and

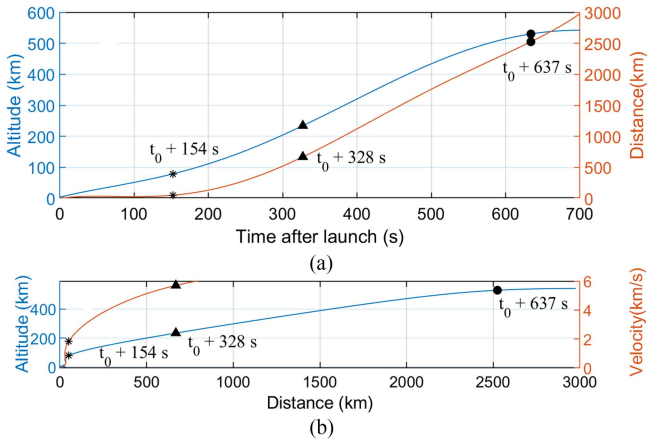

Fig. 12. Schematic diagram of rocket's flight time, altitude, horizontal distance, and flight speed. (a) Blue solid line and red solid line represent the rocket flight altitude and distance as functions of time after the launch, respectively. The black asterisk, black triangle, and circle represent the three moments of first/second stage separation ($t0$ + 154 s), 2nd stage main engine shut down ($t0$ + 328 s), and spacecraft/ LV separation ($t0$ + 637 s), respectively. (b) Blue solid line and red solid line represent the rocket flight altitude and velocity as functions of its distance after the launch, respectively.

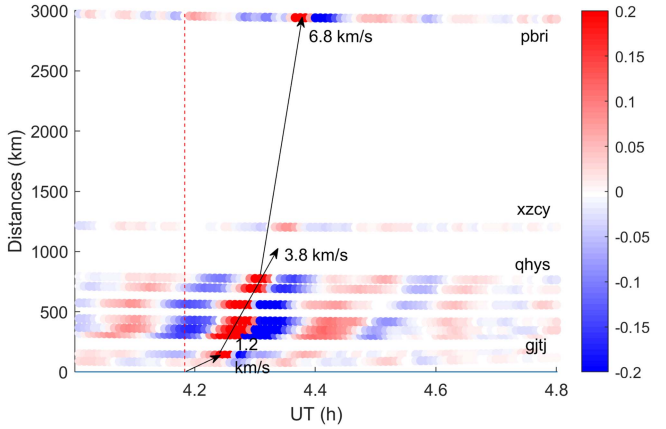

Fig. 13. Schematic diagram of the rocket's flight speed. The slope of the black arrow represents the propagation speed of the shock wave. The colors represent TEC perturbations in TECU.

flight distance (red curve) after launch. Fig. 12(b) shows the relationship between the flight distance, flight altitude (blue curve), and flight speed (red curve) after launch. The black asterisk, the black triangle, and the circle represent three important moments, respectively: the first and second stage separation ($t0$ + 154 s), the second stage shutdown ($t0$ + 328 s), and the separation of the rocket and satellite ($t0$ + 637 s). The LV of this launch event is an SSO satellite, with a flight altitude of ∼500 km. The rocket passes through the D-F2 layer of the ionosphere. Fig. 12 shows that when the rocket is 500 and 1500 km away from the launch site, the flight times are $t0$ + 300 s and $t0$ + 460 s after launch, respectively, and the altitudes reach 200 and 400 km, respectively.

According to Fig. 12, the second stage main engine of the rocket has been shut down ($t0$ + 328 s), the speed has reached 6 km/s, and the distance from the launch site has exceeded 1500 km. The rocket is still rising, and releases most of the thrust when it is in the initial stages of launch ($t0$ + 200 s – $t0$ + 300 s). The rocket flies nearly horizontal at supersonic speed when it is in the middle and late stages of launch ($t0$ + 400 s – $t0$ + 500 s). The excitation source is located in the rocket trajectory, and moves dynamically with the rocket. The engine tail flame of the rocket can no longer produce large acoustic explosion disturbances.

The velocity of the shock wave is 800– 1000 m/s and 2210 m/s in region A and region B are shown in Fig. 6, respectively. In scheme 3, considering the rocket velocity, the horizontal velocity of the shock wave is 1861 m/s in region B. The velocity of the shock wave in region A is coincident with the other research results in the velocity range of 600–1670 m/s [10], [11], [12], [21]. However, the velocity of the shock wave in region B is higher than the previous research results. Only Kakinami et al. [22] who used a dual-frequency GNSS to observe a missile launch in North Korea, calculated a result that exceeded 2000 m/s.

Based on the analysis of previous launch events, it is found that the flight altitude of most of the previous research events is only ∼200 km [4], [5], [6], [8], [10] and that most of the excitation sources of the shock wave are at altitudes of +100 km. In one SSO satellite launch event [12], although the altitude of the rocket reached ∼700 km, the analyzed and calculated IPPs were only ∼1500 km away from the launch site that the rocket flight altitude had still not reached 400 km, i.e., the excitation source of the shock wave had not reached 400 km. Therefore, the propagation speed of the shock wave is slightly higher than that shown in previous studies, which may be owing to the fact that the flight altitude of the rocket in area B exceeds 400 km, and because the propagation speed of a shock wave generated by rocket at a higher atmospheric altitude is higher.

In addition, by calculating the distance from the IPPs to the satellite launch site, the velocity of the rocket can be roughly calculated. Fig. 13 shows the time distance map drawn by the series of satellite G20 observed from the stations of the pink triangle (see Fig. 1), and indirectly reflecting the rocket speed. The mean speeds of the rocket are 1.2, 3.8, and 6.8 km/s at 300 km, 1200 km, and 3000 km from the launch site, respectively, reflecting the gradual acceleration of the rocket. The calculation results are consistent with those in Fig. 12.

B. Depletions

Fig. 11 shows the 2-D distribution of depletion with time. By combining Figs. 11 and 12, the relationships between the time and amplitude of the depletion and the flight time, flight altitude, and flight position of the rocket can be analyzed. The depletion first appears 5 min after the launch, 300 km away from the launch site. At this time, the rocket has achieved first/second stage separation, and the altitude of the rocket is ∼100 km. After that, the depletion gradually increases, and the central area of the depletion is 400 km south of the rocket launch site, reaching the maximum value. With the secondary main engine shut down ($t0$ + 328 s), the distance from the south of the launch site to 700 km along the trajectory is gradually reduced, and the depletion gradually decreases, disappearing after the distance

from the south of the launch site reaches 1000 km. Before the first/second stage separation, the depletion is not evident that the altitude of the rocket does not reach 100 km. After the second stage shutdown of the rocket, the matter ejected into the atmosphere by the rocket decreases, and the depletion gradually decreases.

It is concluded that the formation time of depletion is mainly between the time nodes of the first/second stage separation and the second stage shutdown of the rocket. At this time, the altitude of the rocket reaches 100–300 km, and the rocket is in an accelerating/rising stage, which consumes a significant amount of chemical fuel, and releases a significant amount of combustion propellant into the ionosphere. The combustion of the rocket tail flame reacts with the chemical reactions of other ions in the atmosphere (a large number of H_2O and H_2 ions, and a large number of O^+ ions occupying the F2 layer). Then, these molecular ions combine and react rapidly again in the ionosphere, forming a hole in the ionosphere. The depletion has an amplitude of ∼3.8 TECU, which is smaller than the ∼12 TECU found in other studies [12]. The reason is that the background TEC is only 6.8 TECU, and the reduction ratio of depletion is still 56%, consistent with the previous research results of 50% [23]. In addition to the influence of the amount of combustion gases emitted by different launch missions, the depletion is also related to the TEC value of the background field.

The depletion can last for ∼2 h, longer than found in the previous observation results (i.e., 1 h) [9], [24], [25], but more consistent with the observation results of Liu et al. [12]. The spacecraft orbit altitude of the former is generally less than 200 km, but the latter is similar to this launch mission (SSO), with an altitude of more than 500 km. The main reason is the difference in the amount of propellant consumed by different LVs via injection into the atmosphere, and the altitude of the LV. The key time nodes of the rocket launch are consistent with the amount of propellant consumed by injection into the atmosphere.

In this launch event, the depletion area is roughly symmetrical to the rocket trajectory, which is inconsistent with the observation records, with evident westward deviation [12], [17]. According to the horizonal wind model HWM14, the neutral wind speed in the area with the largest depletion area (400–600 km south of the launch site) is ∼3.6 m/s. Owing to the smaller speed of the background wind, the depletion basically diffuses evenly around the rocket track, without a large deviation. Choi and Kil [17] and Liu et al. [12] used HWM07 and HWM14 models to calculate the wind speed in the depletion area, reaching 120 and 70–90 m/s, respectively. The background wind has a large westward component, so the depletion presents a significant west bias phenomenon. The observation results and wind speed results also support the view that the movement of the depletion may be related to the background winds.

C. Conclusion

In the article, we investigated the effects of the launch of the rocket on the ionosphere. The ionospheric depletions were obtained by a second-order polynomial fitting of the vTEC observations. The depletion main appeared at 300–400 km south of the launch site as the center, and gradually symmetrical spreads around along the rocket trajectory, lasting for ∼2 h. The maximum amplitude of the depletion was ∼3.8 TECU, accounting for 56% of the background value of the TEC. In the process of rocket launching, the large amount of water vapor produced by fuel consumption reacts with other ions in the atmosphere, which is the main cause of ionospheric holes. In addition, the shock wave is obtained by a band-pass filter of the $vTEC_L$ with a high sampling rate of 1 s observations. The shock wave first appeared at 140 km away from the launch site after the launch, and still be observed 3000 km away from the launch site. The average velocity of the shock wave can reach ∼1861 m/s when the shock wave appeared 2200 km away from the launch site at an altitude of more than 400 km. The propagation speed of a shock wave at a higher altitude is higher than at a lower altitude. The excitation source of the shock wave may be the multi-point excitation from the rocket motion, and the supersonic motion of the rocket is the main cause of the shock wave.

ACKNOWLEDGMENT

The authors would like to thank the IGS, GNSS Center at Wuhan University, Yunnan Basic Surveying and Mapping Technology Center, and First Institute of Surveying and Mapping at Qinghai Province for providing the GNSS observations. We are also grateful to the editors and four anonymous reviewers for their careful work and valuable comments that have helped improve this article substantially.

REFERENCES

[1] E. L. Afraimovich, E. A. Kosogorov, K. S. Palamarchouk, N. P. Perevalova, and A. V. Plotnikov, "The use of GPS arrays in detecting the ionospheric response during rocket launchings," *Earth Planets Space*, vol. 52, no. 11, pp. 1061–1066, 2000.

[2] H. G. Booker, "A local reduction of F-region ionization due to missile transit," *J. Geophys. Res.*, vol. 66, no. 4, pp. 1073–1079, 1961.

[3] P. R. Arendt, "Ionospheric undulations following apollo 14 launching," *Nature*, vol. 231, no. 5303, pp. 438–439, 1971.

[4] S. T. Noble, "A large-amplitude traveling ionospheric disturbance excited by the space shuttle during launch," *J. Geophys. Res., Space*, vol. 95, no. A11, pp. 19037–19044, 1990.

[5] Y. Q. Li, A. R. Jacobson, R. C. Carlos, R. S. Massey, Y. N. Taranenko, and G. Wu, "The blast wave of the Shuttle plume at ionospheric heights," *Geophys. Res. Lett.*, vol. 21, pp. 2737–2740, 1994.

[6] E. Calais and J. B. Minster, "GPS, earthquakes, the ionosphere, and the space shuttle," *Phys. Earth Planet. Interiors*, vol. 105, no. 3/4, pp. 167–181, 1998.

[7] E. L. Afraimovich, E. A. Kosogorov, L. A. Leonovich, K. S. Palamartchouk, N. P. Perevalova, and O. M. Pirog, "Observation of large-scale traveling ionospheric disturbances of auroral origin by global GPS networks," *Earth Planets Space*, vol. 52, no. 10, pp. 669–674, 2000.

[8] T. Furuya and K. Heki, "Ionospheric hole behind an ascending rocket observed with a dense GPS array," *Earth Planets Space*, vol. 60, no. 3, pp. 235–239, 2008.

[9] M. Ozeki and K. Heki, "Ionospheric holes made by ballistic missiles from North Korea detected with a Japanese dense GPS array," *J. Geophys. Res., Space*, vol. 115, 2010, Art. no. A9314.

[10] F. Ding et al., "Ionospheric response to the shock and acoustic waves excited by the launch of the Shenzhou 10 spacecraft," *Geophys. Res. Lett.*, vol. 41, no. 10, pp. 3351–3358, 2014.

[11] C. H. Lin et al., "Ionospheric shock waves triggered by rockets," *Ann. Geophys.-Germany*, vol. 32, no. 9, pp. 1145–1152, 2014.

[12] H. Liu et al., "Depletion and traveling ionospheric disturbances generated by two launches of China's long march 4B rocket," *J. Geophys. Res., Space*, vol. 123, no. 12, pp. 310–319, 2018.
[13] T. Bowling, E. Calais, and J. S. Haase, "Detection and modelling of the ionospheric perturbation caused by a space shuttle launch using a network of ground-based global positioning system stations," *Geophys. J. Int.*, vol. 192, pp. 1324–1331, 2013.
[14] E. L. Afraimovich, E. A. Kosogorov, and A. V. Plotnikov, "Shock-acoustic waves generated during rocket launches and Earthquakes," *Cosmic Res.*, vol. 40, pp. 241–254, 2002.
[15] C. C. H. Lin et al., "Concentric traveling ionospheric disturbances triggered by the launch of a spaceX Falcon 9 rocket," *Geophys. Res. Lett.*, vol. 44, pp. 7578–7586, 2017.
[16] M. Mendillo, G. S. Hawkins, and J. A. Klobuchar, "An ionospheric F-region disturbance induced by the launch of Skylab," *Effect Ionosphere Space Syst. Commun.*, p. 205, 1975.
[17] B. Choi and H. Kil, "Large ionospheric TEC depletion induced by the 2016 North Korea rocket," *Adv. Space Res.*, vol. 59, no. 2, pp. 532–541, 2017.
[18] F. Ding, W. Wan, B. Ning, and M. Wang, "Large-scale traveling ionospheric disturbances observed by GPS total electron content during the magnetic storm of 29-30 October 2003," *J. Geophys. Res., Space*, vol. 112, 2007, Art. no. A6309.
[19] T. Ogawa, N. Nishitani, T. Tsugawa, and K. Shiokawa, "Giant ionospheric disturbances observed with the SuperDARN Hokkaido HF radar and GPS network after the 2011 Tohoku earthquake," *Earth Planets Space*, vol. 64, no. 12, pp. 1295–1307, 2012.
[20] A. Saito, S. Fukao, and S. Miyazaki, "High resolution mapping of TEC perturbations with the GSI GPS Network over Japan," *Geophys. Res. Lett.*, vol. 25, pp. 3079–3082, 1998.
[21] E. Calais and J. B. Minster, "GPS detection of ionospheric perturbations following a space shuttle ascent," *Geophys. Res. Lett.*, vol. 23, pp. 1897–1900, 1996.
[22] Y. Kakinami et al., "Ionospheric disturbances induced by a missile launched from North Korea on 12 December 2012," *J. Geophys. Res., Space*, vol. 118, pp. 5184–5189, 2013.
[23] J. Zinn and C. D. Sutherland, "Effects of rocket exhaust products in the thermosphere and ionosphere," 1980.
[24] N. Yuki and H. Kosuke, "Ionospheric hole made by the 2012 North Korean rocket observed with a dense GNSS array in Japan," *Radio Sci.*, vol. 49, no. 7, pp. 497–505, 2014.
[25] L. M. He, L. X. Wu, S. J. Liu, and S. N. Liu, "Superimposed disturbance in the ionosphere triggered by spacecraft launches in China," *Ann. Geophys.-Germany*, vol. 33, pp. 1361–1368, 2015.

Youkun Wang received the M.S. degree in geodesy and surveying engineering from the Faculty of Land Resources Engineering, Kunming University of Technology, Kunming, China, in 2008. He is currently working toward the Ph.D. degree with the School of Geodesy and Geomatics, Wuhan University, Wuhan, China.

His main research interests include GNSS data processing, ionospheric disturbances analysis, and ionospheric modeling.

Yibin Yao received the B.S., M.S., and Ph.D. degrees in geodesy and surveying engineering from Wuhan University, Wuhan, China, in 1997, 2000, and 2004, respectively.

He is currently a Professor with Wuhan University, Wuhan, China. His research interests include ionospheric/tropospheric studies, and high-precision GNSS data processing.

Jian Kong received the B.S. degree from the Shandong University of Science and Technology, Qingdao, China, in 2009, and the Ph.D. degree from the School of Geodesy and Geomatics, Wuhan University, Wuhan, China, in 2014, both in geodesy and surveying engineering.

His research interests include GNSS data processing, global ionospheric modeling using multi-source geodesy observations, 3-D ionospheric tomography based on GNSS observations, and ionospheric anomalies analysis under abnormal conditions.

Lulu Shan received the M.S. degree in geodesy and surveying engineering in 2019 from the School of Geodesy and Geomatics, Wuhan University, Wuhan, China, where she is currently working toward the Ph.D. degree.

Her main research interests include GNSS data processing, GNSS Space Environment Science, ionospheric disturbances analysis under abnormal conditions, and the coupling between ionosphere and lower atmosphere.